Available online at www.sciencedirect.com
SCIENCE DIRECT®
Geoderma 134 (2006) 240–252
GEODERMA
www.elsevier.com/locate/geoderma

Multifractal Sierpinski carpets: Theory and application to upscaling effective saturated hydraulic conductivity

E. Perfect [a,*], R.W. Gentry [b], M.C. Sukop [c], J.E. Lawson [a]

[a] Department of Earth and Planetary Sciences, University of Tennessee, Knoxville, TN 37996-1410, USA
[b] Department of Civil and Environmental Engineering, University of Tennessee, Knoxville, TN 37996-2010, USA
[c] Department of Earth Sciences, Florida International University, Miami, Fl 33199, USA

Available online 19 April 2006

Abstract

Recent analyses of field data suggest that saturated hydraulic conductivity, K, distributions of rocks and soils are multifractal in nature. Most previous attempts at generating multifractal K fields for flow and transport simulations have focused on stochastic approaches. Geometrical multifractals, in contrast, are grid-based and thus better able to simulate distinct facies or horizons. We present a theoretical framework for generating two-dimensional geometrical multifractal K fields. Construction of monofractal Sierpinski carpets using the homogenous and heterogeneous algorithms is recalled. Averaging multiple, non-spatially randomized, heterogeneous Sierpinski carpet generators yields a new generator with variable mass fractions determined by the truncated binomial probability distribution. Repeated application of this generator onto itself results in a multiplicative cascade of mass fractions or multifractal. The generalized moments, $M_i(q)$, of these structures scale as $M_i(q)=(1/b^i)^{(q-1)Dq}$, where b is the scale factor, i is the iteration level and D_q is the q−th order generalized dimension, with q being any integer between $-\infty$ and ∞. This theoretical approach is applied to the problem of aquifer heterogeneity by equating the mass fractions with K. An approximate analytical expression is derived for the effective hydraulic conductivity, K_{eff}, of multifractal K fields, and K_{eff} is shown to increase as a function of increasing length scale in power law fashion, with an exponent determined by $D_{q\to\infty}$. Numerical simulations of flow in $b=3$, $D_{q\to\infty}=1.878$ and $i=1$ though 5 multifractal K fields produced similar increases in K_{eff} with increasing length scale. Extension of this approach to three dimensions appears to be relatively straightforward.
© 2006 Elsevier B.V. All rights reserved.

1. Introduction

How to describe, predict and simulate heterogeneity are pervasive issues in the fields of hydrogeology, petroleum engineering, and soil physics. Heterogeneities can occur in chemical and physical properties, both spatially and temporally. We are concerned with the spatial variation in physical properties, specifically the saturated hydraulic conductivity, K, of different geological facies or soil horizons. Such variations impact flow and transport in the subsurface, and thus have practical significance for the design and operation of pumping wells for human water use, oil production, and the spreading of contaminants in polluted soils and aquifers.

Increasingly, fractal-based models are being used to describe, predict and simulate aquifer heterogeneity (see for example the recent reviews by Neuman and Di Federico, 2003; Molz et al., 2004). Fractals are spatial or temporal patterns that repeat themselves at increasingly finer (or coarser) scales of resolution (Mandlebrot,

* Corresponding author. Tel.: +1 865 974 6017; fax: +1 865 974 2368.
E-mail address: eperfect@utk.edu (E. Perfect).

0016-7061/$ - see front matter © 2006 Elsevier B.V. All rights reserved.
doi:10.1016/j.geoderma.2006.03.001

1982; Gouyet, 1996). The focus of this work is on two-dimensional spatial patterns constructed from a solid starting mass by an iterative process of mass removal and re-scaling.

As a concrete example, consider the Sierpinski carpet (named after the Polish mathematician Waclaw Sierpinski, 1882–1969) in Fig. 1. Construction based on the homogenous algorithm begins with a solid square of unit length (the *initiator*), which is divided into b^2 smaller squares of length $1/b$, where $b=2,3,4\ldots$ is a scale factor. At the first iteration level ($i=1$), n smaller squares are removed. In Fig. 1, $b=3$ and $n=1$. In subsequent iterations, this *generator* (Fig. 1A) is scaled down and applied to the remaining parts. In general, the number of remaining parts of length $1/b^i$ is given by $N(1/b^i)=(1/b^i)^{-D}$, where D is the mass fractal dimension defined as:

$$D \equiv \log(b^2-n)/\log(b) \quad (1)$$

For the example in Fig. 1, $D=1.892\ldots$ resulting in $N(1/3^1)=8$ for the first iteration, $N(1/3^2)=64$ for the second iteration and so on; the carpet produced after five iteration levels is shown in Fig. 1B.

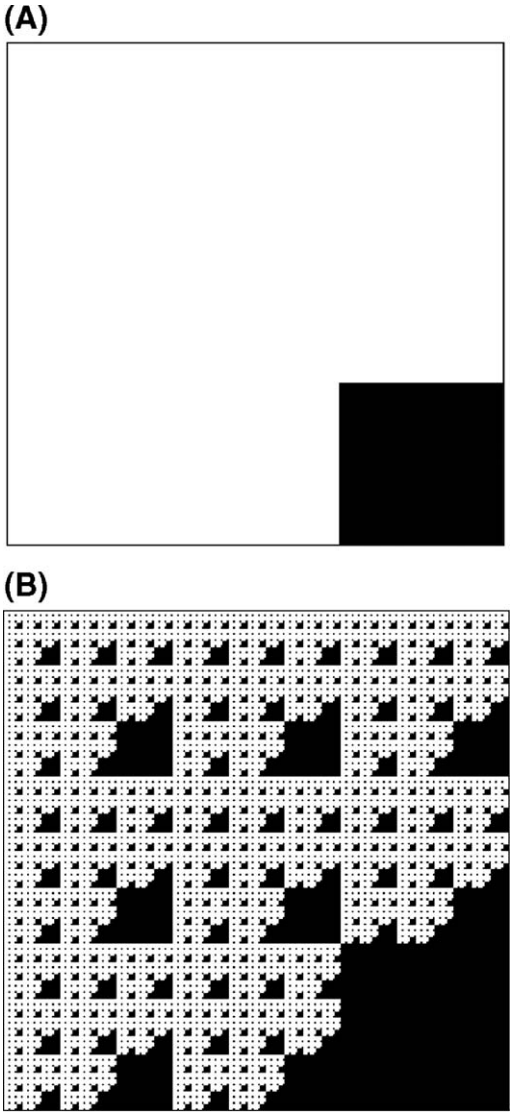

Fig. 1. Monofractal Sierpinski carpet with $p=8/9$ and $b=3$: (A) $i=1$ (generator) and (B) $i=5$. Remaining parts=white, removed parts=black.

The Sierpinski carpet and its three-dimensional cousin, the Menger sponge, have a long history of applications to natural porous media. They have primarily been used as models for pore spaces (Garrison et al., 1992, 1993) and fracture networks (Doughty and Karasaki, 2002) in rocks and soils. The percolation thresholds of randomized Sierpinski carpets were investigated by Sukop et al. (2002). In vadose zone applications, these fractals are often invoked in physically based derivations of the capillary pressure–saturation relation (Tyler and Wheatcraft, 1990; Bird et al., 1996; Perfect, 2005). Bird and Dexter (1997) and Sukop et al. (2001) studied the drainage characteristics of randomized Sierpinski carpets using a numerical invasion percolation algorithm. In an early application to aquifer heterogeneity, Wheatcraft et al. (1991) conducted numerical saturated flow and transport simulations in Sierpinski carpets; the carpets were used as a spatial model for facies with a bimodal K distribution.

More recently, detailed analyses of large data sets have revealed that K distributions of sedimentary rocks (Liu and Molz, 1997; Boufadel et al., 2000; Tennekoon et al., 2003) and soils (Giménez et al., 1999) are multifractal in nature. As will be explained in the next section, multifractals are characterized by a range of D values instead of a single fractal dimension, as is the case for the monofractal Sierpinski carpets discussed previously. Most attempts at generating multifractal K fields have concentrated on stochastic approaches (Boufadel et al., 2000; Tennekoon et al., 2003; Veneziano and Essiam, 2003). Numerical simulations of flow and transport in such fields have been reported by Veneziano and Essiam (2003, 2004). Numerical flow and transport simulations have also been performed in quasi-multifractal K fields generated with an algorithm based on bounded fractional Lévy motion (Painter and Mahinthakumar, 1999).

Compared to stochastic multifractals and Lévy motions, geometrical multifractals are grid-based and thus better able to simulate the spatial variability of K as a function of distinct geological facies or soil horizons.

Furthermore, they are computationally very easy to generate. Saucier (1992a,b) used geometrical multifractals, combined with real space renormalization group (RG) theory, to derive the following analytical expression for the effective normalized permeability, K_{eff}, as a function of carpet/aquifer size:

$$K_{\text{eff}} = \left(\frac{1}{b^i}\right)^{\gamma} \tag{2}$$

In Eq. (2), $\gamma = \log_b[f(f_{1,1}, f_{2,1}, \ldots, f_{j,1})]$, where f is an undefined function, $f_{j,1}$ is the j−th mass fraction of the generator ($i=1$), and $1 \le j \le b^2$ is a counting index. Values of $f_{j,1}$ were chosen arbitrarily under the condition that $\sum_{j=1}^{b^E} f_{j,1} = 1$. Mukhopadhyay and Sahimi (2000) also employed the RG method, along with an effective medium approximation, to compute the K_{eff} of geometrical multifractal permeability fields. However, these authors did not relate their results to the parameters used to generate the multifractal fields.

The objectives of this paper are: (i) to present a general theoretical framework for generating geometrical multifractal Sierpinski carpets, (ii) to compute the generalized dimensions for such carpets, (iii) to apply these results to the problem of aquifer heterogeneity by deriving an analytical expression for K_{eff} and (iv) to test this expression against numerical simulations of flow performed in multifractal Sierpinski carpets.

2. Theory

2.1. Mass fractions

The mass fraction associated with the j−th part of a homogeneous Sierpinski carpet at the i−th iteration level, $f_{j,i}$, is given by:

$$f_{j,i} = \frac{1}{N(1/b^i)} = \left(b^i\right)^{-D}, \qquad 1 \le j \le \left(b^i\right)^D \tag{3a}$$

$$f_{j,i} = 0, \qquad \left(b^i\right)^D < j \le (b^i)^2 \tag{3b}$$

Note that, for any given iteration level, the mass fractions always sum to one. For the Sierpinski carpet generator in Fig. 1, it follows that the mass, $f_{j,1}$, will be distributed among the $j=3^2$ parts as indicated in Fig. 2A. Combining Eqs. (1) and (3a,b) leads to an alternative definition of the mass fractal dimension based on the generator mass fractions, i.e.

$$D \equiv -\log(f_{j,1})/\log(b), \qquad f_{j,1} > 0 \tag{4}$$

2.2. Heterogeneous algorithm

Sierpinski carpets can also be generated probabilistically using the following heterogeneous algorithm (Mandlebrot, 1982; Gouyet, 1996):

- Divide initiator into b^2 parts
- Choose probability p ($\equiv 1 - n/b^2$) that $b^2 - n$ parts remain
- For each part, generate a uniformly distributed random number in the interval [0,1]
- If the random number is greater than p, remove that part

Let us consider the behavior of this algorithm. Say that we wish to generate a probabilistic version of the Sierpinski carpet in Fig. 1. Hence, $p=8/9$ (=0.888...). We generate three realizations of $b^2=9$ random numbers and show them in Table 1. It is clear from Table 1 that the heterogeneous algorithm sometimes fails to retain the correct number of parts (i.e., 8 for the homogenous Sierpinski carpet) needed to satisfy the simple fractal scaling law $N(1/b^i)=(1/b^i)^{-D}$; for example, $N=9$ and $N=7$ in the second and third realizations, respectively. The corresponding fractal dimensions, based on either Eq. (1) or Eq. (4), are $D=1.771\ldots$ and $D=2.000$, respectively, rather than $D=1.892\ldots$ as is characteristic of the homogeneous Sierpinski carpet. Although D may vary with each realization of the heterogeneous algorithm, it converges to the correct value as $i \to \infty$.

(A)

0.125	0.125	0.125
0.125	0.125	0.125
0.125	0.125	0

(B)

0.127	0.127	0.127
0.127	0.124	0.115
0.127	0.087	0.038

Fig. 2. Generator average mass fractions for $p=8/9$ and $b=3$: (A) monofractal Sierpinski carpet and (B) multifractal Sierpinski carpet.

2.3. Binomial distribution

The decision to retain individual parts in the construction of the carpet is based on independent Bernoulli trials. The problem is the same as asking "What is the probability of obtaining N heads in b^2 flips of an unbalanced coin?" We set the degree of imbalance as the cutoff p; that is, we decide that, if a random number in [0,1] is greater than p, we have a head. The probability of each possible outcome ($N=0, 1, \ldots, b^2$) can then be computed directly from the binomial distribution. Following Freund (1971), we have:

$$B\left(N, b^2, p\right) = \left(\frac{b^2!}{N!(b^2-N)!}\right) p^N \left(1-p\right)^{b^2-N} \tag{5}$$

where $B(N,b^2,p)$ is the binomial probability of N retained parts in a b^2 generator at the selected probability p.

Table 1
Three realizations of nine random numbers in [0,1]

Realization	Random numbers in [0,1]									N[a]
1	0.585	0.811	<u>0.989</u>[b]	0.732	0.761	0.674	0.613	0.877	0.790	8
2	0.488	0.094	0.221	0.667	0.448	0.833	0.636	0.212	0.002	9
3	<u>0.943</u>	0.103	0.878	0.683	0.516	0.171	0.517	<u>0.916</u>	0.516	7

[a] N denotes the number of parts remaining in the generator.
[b] Values greater than $p=8/9$ are underlined.

Fig. 3 shows analytical distributions for the number of parts retained in a heterogeneous Sierpinski carpet as a function of p calculated using Eq. (5). These distributions are discrete and are shown as curves only for clarity. Similar distributions could be determined empirically from multiple realizations of the heterogeneous algorithm. Use of Eq. (5), however, allows computation of the exact probabilities of relatively infrequent occurrences that cannot be readily determined from a sample of realizations. Indeed, focusing on the $p=8/9$ case for example, the instances of 3, 2, 1 or 0 parts retained have probabilities of 1.1×10^{-4}, 5.9×10^{-6}, 1.8×10^{-7} and 2.6×10^{-9}, respectively. Table 1 contains only three realizations so it is not surprising that none of these possibilities occurred. Such small probabilities attest to the near-impossibility of relying on multiple realizations to generate an empirical distribution; more than one billion realizations would be required to adequately sample the probability of occurrence.

2.4. Truncated binomial distribution

Based on the binomial distribution, any given realization of the heterogeneous algorithm can result in $N=0$. If this event occurs in the generator, the Sierpinski carpet would entirely disappear. The fractal dimension is undefined for such a situation. The binomial probabilities for $N=0$ when $b=3$ are given in Table 2. The possibility of retaining zero parts increases dramatically for small values of p.

One way to avoid this difficulty is to constrain the possible values of N to exclude zero. This constraint on the binomial distribution has appeared in other contexts as the truncated binomial distribution (Patil, 1962). The formula for computing the truncated binomial distribution is:

$$B_T\left(N,b^2,p\right)=\frac{\left(\frac{b^2!}{N!(b^2-N)!}\right)p^N(1-p)^{b^2-N}}{\sum_{N=1}^{b^2}\left(\frac{b^2!}{N!(b^2-N)!}\right)p^N(1-p)^{b^2-N}} \tag{6}$$

where $B_T(N,b^2,p)$ is the truncated binomial probability of N retained parts in a b^2 generator given a selected probability p. The summation in the denominator excludes $N=0$ and normalizes the probability density to one. This distribution is also shown in Fig. 3. The deviation from the binomial distribution is large for $p=0/9$ and $p=1/9$. The difference between the distributions gets smaller as p increases and is insignificant for $p\geq4/9$. The multifractal considerations

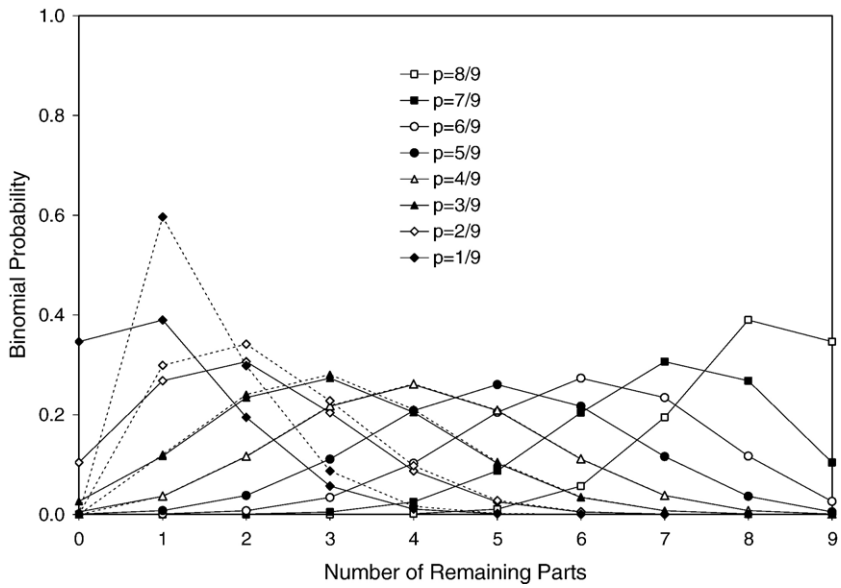

Fig. 3. Binomial, $B(N,b^2,p)$, (solid lines) and truncated binomial, $B_T(N,b^2,p)$, (dashed lines) probability distributions for the number of remaining parts, N, as a function of selected probability, p, for $b=3$ Sierpinski carpet generators. Note that $B(0,9,0/9)=1$, $B_T(0,9,0/9)=0$, $B(9,9,9/9)=1$ and $B_T(9,9,9/9)=1$.

Table 2
Binomial probabilities for $b=3$ and $N=0$ and corresponding sums of average mass fractions

p	$B(0,9,p)$	$\sum_{j=1}^{9}\langle f_{j,1}\rangle$
1/9	0.346	0.654
2/9	0.104	0.896
3/9	0.026	0.974
4/9	0.005	0.995
5/9	6.8×10^{-4}	0.999
6/9	5.1×10^{-5}	1.000
7/9	1.3×10^{-6}	1.000
8/9	2.6×10^{-9}	1.000

below use the truncated binomial distribution. Despite the simplicity of the required modifications, no previous implementations of this approach are known to exist.

2.5. Multifractal Sierpinski carpets

Averaging the mass fractions from multiple, non-spatially randomized, realizations of the heterogeneous algorithm at $i=1$ gives:

$$\langle f_{j,1}\rangle = \sum_{k=0}^{j-1} B_T\left(b^2-k, b^2, p\right)\frac{1}{b^2-k} \tag{7}$$

where $\langle f_{j,1}\rangle$ is the average mass fraction associated with the j−th part of the generator, $1\le j\le b^2$, and k is a counting index. The average mass fractions computed with Eq. (7) always sum to unity. This is in contrast to $\langle f_{j,1}\rangle$ values based on the binomial distribution, which do not always sum to unity because of the increased likelihood of $N=0$ at low p (Table 2).

The average mass fractions obtained by setting $b=3$ and $p=8/9$ in Eq. (7) are shown in Fig. 2B. As compared to the monofractal generator (Fig. 2A), the mass is spread out among all b^2 parts of the generator. The repeated application of the generator described by Eq. (7) onto itself results in a multiplicative cascade of mass fractions or *multifractal* (Gouyet, 1996; Saucier, 1996). Mandelbrot (1974; Mandlebrot, 1982) called this process "canonical curdling". For $i>1$, the average mass fraction in the j−th cell of this iterated function system (IFS) is given by:

$$\langle f_{j,i}\rangle = \langle f_{j,i-1}\rangle \times \langle f_{j,i-1}\rangle \tag{8}$$

where $\langle f_{j,i}\rangle$ and $\langle f_{j,i-1}\rangle$ are the average mass fractions at the i−th and $i-1$−th levels, respectively, and $1\le j\le (b^i)^2$. From Eq. (8), the maximum, $\langle f_{\max,i}\rangle$, and minimum, $\langle f_{\min,i}\rangle$, average mass fractions at the i−th iteration level are $\langle f_{1,i}\rangle^i$ and $\langle f_{(b^i)^2,i}\rangle^i$, respectively. Consider, for example, the generator shown in Fig. 2B; based on Eq. (8), the $j=1$ cell from $i=1$ is sub-divided into nine smaller cells containing the following average mass fractions at $i=2$: $\begin{bmatrix} 0.127\times0.127 & 0.127\times0.127 & 0.127\times0.127 \\ 0.127\times0.127 & 0.127\times0.124 & 0.127\times0.115 \\ 0.127\times0.127 & 0.127\times0.087 & 0.127\times0.038 \end{bmatrix}$. Similarly, the $j=9$ cell from $i=1$ yields: $\begin{bmatrix} 0.038\times0.127 & 0.038\times0.127 & 0.038\times0.127 \\ 0.038\times0.127 & 0.038\times0.124 & 0.038\times0.115 \\ 0.038\times0.127 & 0.038\times0.087 & 0.038\times0.038 \end{bmatrix}$ at $i=2$. It follows that the maximum and minimum average mass fractions at $i=2$ are $\langle f_{\max,i}\rangle=0.127^2$ and $\langle f_{\min,i}\rangle=0.038^2$, respectively. The multifractal Sierpinski carpet resulting from this IFS is illustrated in Fig. 4 for the $i=1$ and $i=5$ iteration levels. Compared to the monofractal carpet (Fig. 1), the mass fractions exhibit increasing variety, as indicated by the wider range of shades of gray present, with increasing iteration level. This is a characteristic of multifractals.

The distribution of $\langle f_{j,1}\rangle$ values in a multifractal generator is usually chosen arbitrarily (e.g., Saucier, 1992a,b, 1996). The approach considered here, however, results in a multifractal generator in which the distribution of $\langle f_{j,1}\rangle$ values depends explicitly on b and p, in a way that does not appear to have been recognized previously.

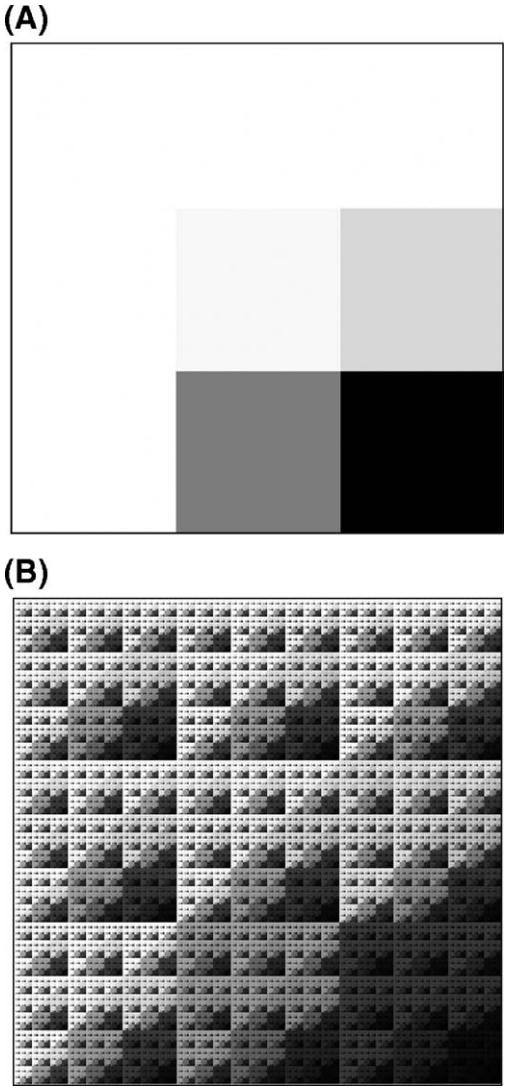

Fig. 4. Multifractal Sierpinski carpet with $p=8/9$ and $b=3$: (A) $i=1$ (generator) and (B) $i=5$. $\langle f_{\min,i}\rangle$ = white, $\langle f_{\max,i}\rangle$ = black.

2.6. Generalized dimensions

Multifractals no longer possess global scale-invariance and instead of being well characterized by a single fractal dimension require a spectrum of generalized dimensions for their description (Mandelbrot, 1989; Evertsz and Mandelbrot, 1992). Here, we compute generalized dimensions for the multifractal Sierpinski carpets discussed above. Although valid for any iteration level, the approach outlined below is particularly useful since it is based on the generator average mass fractions, $\langle f_{j,1}\rangle$.

We first calculate the generalized moments for the generator using the expression (Gouyet, 1996; Turcotte, 1997):

$$M_1(q) = \sum_{j=1}^{b^2} \langle f_{j,1}\rangle^q \tag{9}$$

where $M_1(q)$ is the generalized moment of order q for $i=1$, with q being any integer between $-\infty$ and ∞. The Rényi or q−th order generalized dimension, D_q, is then defined by (Gouyet, 1996; Turcotte, 1997):

$$M_i(q) = \left(\frac{1}{b^i}\right)^{(q-1)D_q} \tag{10}$$

Setting $i=1$ in Eq. (10) and rearranging gives:

$$D_q = \frac{1}{q-1}\log\left(M_1(q)^{-1}\right)/\log(b), \qquad q \neq 1 \tag{11}$$

This result can be used directly as long as $q \neq 1$. The following expression, the derivation of which can be found in Gouyet (1996), is used to compute D_q for $q=1$:

$$D_1 = -\sum_{j=1}^{b^2} \langle f_{j,1}\rangle \log(\langle f_{j,1}\rangle)/\log(b) \tag{12}$$

where D_1 is called the entropy or information dimension. Eq. (12) is based solely on $\langle f_{j,1}\rangle$ and b. By substituting Eq. (9) into Eq. (11), the D_q for $q \neq 1$ can also be calculated using just $\langle f_{j,1}\rangle$ and b. Since $\langle f_{j,1}\rangle$ is given by Eq. (7), this means the entire D_q versus q curve for a multifractal Sierpinski carpet can be predicted from the parameters b and p. If all the values of D_q are equal, a monofractal is defined. If, however, the values of D_q are different, then a multifractal spectrum is defined.

Use of the above equations to calculate the generalized dimensions for $b=3$ and $p=8/9$ Sierpinski carpets is illustrated in Fig. 5. The generator mass fractions employed in these computations are those given in Fig. 2. It can be seen that the monofractal generator produces a straight line that is independent of q and equal to $D_q = D = \log(8)/\log(3)$. In contrast, the multifractal generator produces a smooth non-linear D_q function that passes through two at $q=0$ and approaches minimum and maximum values as $q \rightarrow \pm\infty$, respectively. The minimum D_q for the multifractal is less than D for the monofractal (i.e. $D_{q\rightarrow\infty}=1.878$ versus $D=1.892$).

Fig. 6 shows the calculated generalized dimensions for $b=3$ multifractal Sierpinski carpets with different p values. All of the $D_q=2$ when $q=0$. The D_q versus q functions are much more sensitive to changes in p when q is negative than when it is positive. The D_q maxima decrease with increasing p, while the minima increase.

Following Cawley and Mauldin (1992) and Beck and Schlögl (1993), we calculate the D_q maxima, $D_{q\rightarrow-\infty}$, and minima, $D_{q\rightarrow\infty}$, from the minimum, $\langle f_{\min,1}\rangle$, and maximum, $\langle f_{\max,1}\rangle$, generator average mass fractions respectively, using the expressions:

$$D_{q\rightarrow-\infty} = -\log(\langle f_{\min,1}\rangle)/\log(b) \tag{13a}$$

$$D_{q\rightarrow\infty} = -\log(\langle f_{\max,1}\rangle)/\log(b) \tag{13b}$$

where $\langle f_{\min,1}\rangle = B_T(b^2, b^2, p)\frac{1}{b^2}$ and $\langle f_{\max,1}\rangle = \sum_{k=1}^{b^2} B_T(k, b^2, p)\frac{1}{k}$. As $q \rightarrow -\infty$, the generalized dimensions are dominated by the contribution of the smallest average mass fraction in the generator. Similarly, as $q \rightarrow \infty$, the

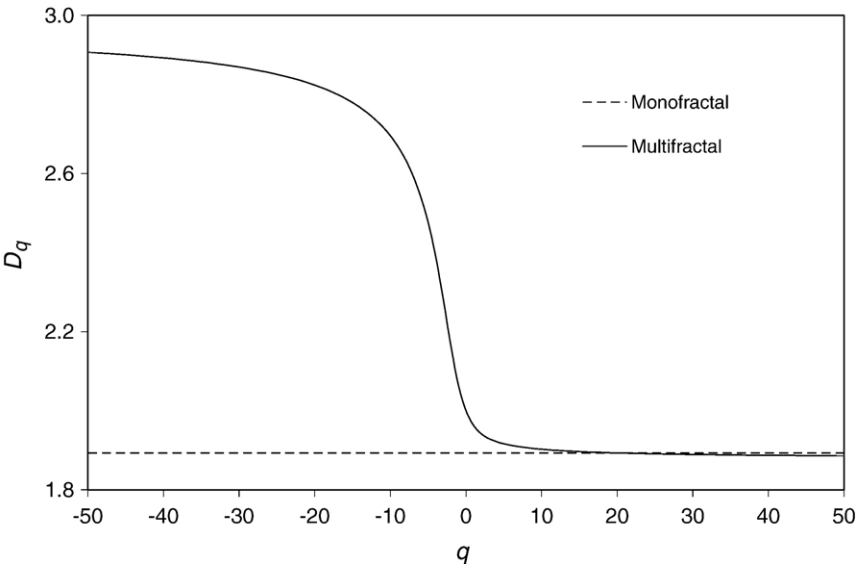

Fig. 5. Generalized dimensions versus q for monofractal and multifractal Sierpinski carpets with $p=8/9$ and $b=3$.

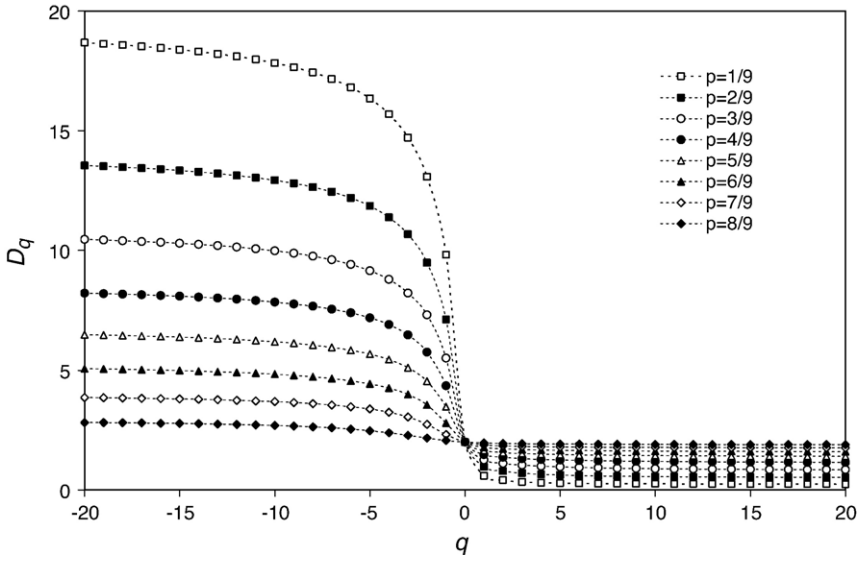

Fig. 6. Generalized dimensions versus q for $b=3$ multifractal Sierpinski carpets with different p values.

generalized dimensions are determined by the largest generator average mass fraction. Values of $\langle f_{\min,1}\rangle$, $\langle f_{\max,1}\rangle$, $D_{q\to-\infty}$ and $D_{q\to\infty}$ calculated using Eqs. (7) and (13a, b) are listed in Table 3 for $b=3$ multifractal Sierpinski carpets with different p values. With the sole exception of $p=1/9$, the $D_{q\to\infty}$ values in Table 3 are less than the corresponding D values for monofractal Sierpinski carpets calculated using Eq. (1). For $p<8/9$, the $D_{q\to-\infty}$ values in Table 3 are all greater than 3. While mathematically permissible, the physical meaning such values is unclear.

3. Materials and methods

Five iterations of the $b=3$ and $p=8/9$ monofractal and multifractal Sierpinski carpets visualized in Figs. 1 and 4 were generated, resulting in 9, 81, 729, 6561 and 59,049 average mass fractions for the $i=1$, 2, 3, 4 and 5 iteration levels, respectively. The average mass fractions were normalized using the equation:

$$f_{j,i}^{*}=\frac{\langle f_{j,i}\rangle-\langle f_{\min,i}\rangle}{\langle f_{\max,i}\rangle-\langle f_{\min,i}\rangle} \tag{14}$$

where $f_{j,i}^{*}$ is the normalized average mass fraction of the j −th part at the i−th iteration level, and $\langle f_{\min,i}\rangle$ and $\langle f_{\max,i}\rangle$ are the minimum and maximum average mass fractions at the i−th iteration level, respectively.

The normalized mass fractions were converted into two-dimensional saturated hydraulic conductivity fields by assuming $K_{j,i}\propto f_{j,i}^{*}$, where $K_{j,i}$ is the saturated hydraulic conductivity of the j−th part at the i-th iteration level, i.e.

$$K_{j,i}=(K_{\max}-K_{\min})f_{j,i}^{*}+K_{\min} \tag{15}$$

where $K_{\max}$ and $K_{\min}$ are the maximum and minimum hydraulic conductivities, respectively. Note that, in Eq.

Table 3
Monofractal D values, and maximum and minimum average mass fractions for $b=3$ and $i=1$ multifractal Sierpinski carpets, along with corresponding generalized dimensions in the limits $q\to-\infty$ and $q\to\infty$

P	D	$\langle f_{\min,1}\rangle$	$\langle f_{\max,1}\rangle$	$D_{q\to-\infty}$	$D_{q\to\infty}$
1/9	0.000	4.388×10^{-10}	0.778	19.613	0.227
2/9	0.631	1.639×10^{-7}	0.577	14.222	0.501
3/9	1.000	5.796×10^{-6}	0.414	10.976	0.802
4/9	1.262	7.556×10^{-5}	0.300	8.639	1.097
5/9	1.465	5.605×10^{-4}	0.226	6.815	1.355
6/9	1.631	0.003	0.179	5.322	1.566
7/9	1.771	0.012	0.148	4.059	1.736
8/9	1.893	0.038	0.127	2.965	1.878

(15), $K_{j,i} \rightarrow K_{\min}$ as $f_{j,i}^* \rightarrow 0$ and $K_{j,i} \rightarrow K_{\max}$ as $f_{j,i}^* \rightarrow 1$. An effective hydraulic conductivity for the i−th level field, $K_{\text{eff},i}$, was then calculated using the expression:

$$K_{\text{eff},i} = \langle K_{j,i} \rangle = \langle (K_{\max} - K_{\min}) f_{j,i}^* + K_{\min} \rangle = (K_{\max} - K_{\min}) \langle f_{j,i}^* \rangle + K_{\min} \quad (16)$$

where $\langle\rangle$ denotes the arithmetic average, with $\langle f_{j,i}^* \rangle$ being the mean of the normalized mass fractions. For simplicity, we assumed $K_{\min}=0$ and $K_{\max}=1$ in this study (i.e., $K_{j,i}=f_{j,i}^*$ and $K_{\text{eff},i}=\langle f_{j,i}^* \rangle$). The geometric, harmonic and perturbation method means of the $K_{j,i}$ fields were also computed for comparative purposes using standard formulae (King, 1989; Renard and de Marsily, 1997).

A unit cube aquifer was used for the numerical simulations. The boundary conditions were implemented with constant head (unit gradient) parallel planes, and corresponding zero flux planes on the normal axes. Because the multifractal carpets were slightly asymmetric (Fig. 4), two cases were considered with the gradient applied along the x- and y-axes, respectively. To permit comparisons among iteration levels, the $i=1$ through 4 constructions were further sub-divided so that all the grid sizes were equal to the $i=5$ level. Discretized hydraulic conductivities were assigned based on the normalized mass fractions. Pre- and post-processing of the model realizations were performed using Argus Open Numerical Environments (Argus ONE; Shapiro et al., 1997). The domain was discretized using a block center grid consisting of 59,049 uniformly spaced nodes. A finite difference simulation model based on MODFLOW 2000 (Harbaugh et al., 2000) was used. "Zone budget" was employed to calculate the flow balance into and out of the reservoir (Harbaugh, 1990). The discharge into and out of the unit cube, under a unit gradient, was then used to calculate $K_{\text{eff},i}$ based on Darcy's law (Renard and de Marsily, 1997).

4. Results and discussion

The results of the numerical simulations are shown in Fig. 7. The effective saturated hydraulic conductivities decreased with increasing iteration level. Because of the slight asymmetry in the multifractal fields (Fig. 4), the numerical $K_{\text{eff},i}$ values for the x-direction were between 6.0% and 9.5% lower than corresponding values for the y-direction.

Regardless of the iteration level, effective saturated hydraulic conductivities based on the arithmetic, geometric, harmonic and perturbation method means always ranked in the order: harmonic < geometric < perturbation method < arithmetic. The same ranking was also observed by King (1989) for an aquifer with a uniform permeability

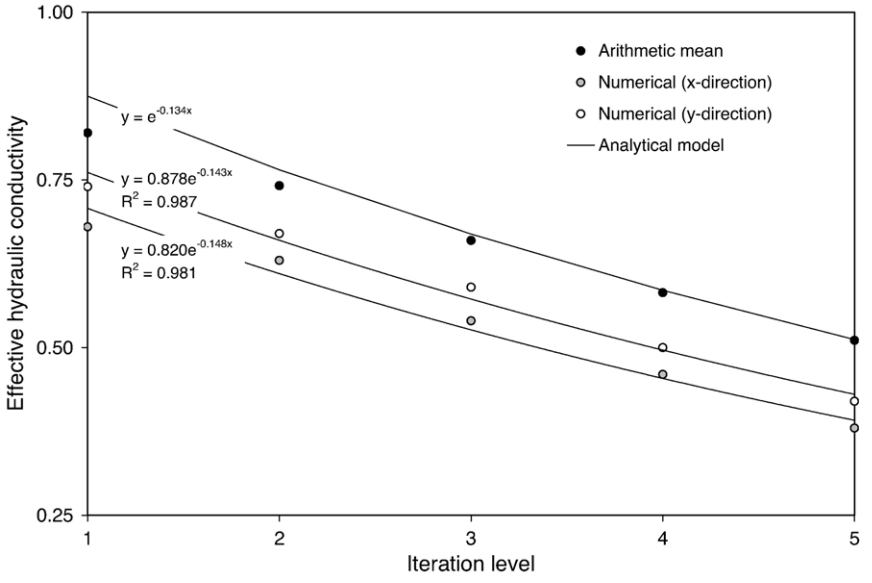

Fig. 7. Effective hydraulic conductivity as a function of iteration level for $p=8/9$ and $b=3$ multifractal Sierpinski carpets.

distribution. Effective saturated hydraulic conductivities from the numerical simulations were most closely related (in terms of slope and coefficient of determination) to the arithmetic means of the multifractal fields (Table 4). As a result, only the arithmetic averaging procedure will be discussed further.

The arithmetic mean of a multifractal field is given by the following approximate analytical expression:

$$K_{\text{eff}} = \langle f^* \rangle = \frac{\left(\frac{1}{b^2}\right)^i - \left(B_T(b^2, b^2, p) \cdot \frac{1}{b^2}\right)^i}{\left(\sum_{k=1}^{b^2} B_T(k, b^2, p) \cdot \frac{1}{k}\right)^i - \left(B_T(b^2, b^2, p) \cdot \frac{1}{b^2}\right)^i} \approx e^{-\alpha i}, \; i \gg 0 \tag{17}$$

where $\alpha = \ln\left(b^2 \cdot \left(\sum_{k=1}^{b^2} B_T(k, b^2, p) \cdot \frac{1}{k}\right)\right) = \ln\left(b^2 \cdot \langle f_{\max,1} \rangle\right)$. Eq. (17) does a good job of predicting the actual decrease in arithmetic $K_{\text{eff},i}$ values with increasing i-level after about three iterations (Fig. 7). Although different in overall magnitude, the numerical $K_{\text{eff},i}$ values decreased with increasing iterations in a qualitatively similar way to that predicted by Eq. (17). Introducing an additional fitting parameter to account for this offset, nonlinear regression analyses (Fig. 7) yielded estimates of α from the numerical simulations that were within 10% ($\alpha = 0.148$ and 0.143 for the x- and y-flow directions, respectively) of the predicted value ($\alpha = 0.134$) based on $p = 8/9$ and $b = 3$ for these fields. Further research on multifractal K fields with different p and b values, and constructed to higher iteration levels, is needed to fully test the predictive capability of Eq. (17).

A relationship between $K_{\text{eff},i}$ and the iteration level automatically implies that $K_{\text{eff},i}$ is scale-dependent. Under field conditions, it is well known that the mean value of saturated hydraulic conductivity estimates increases with the scale of observation or resolution (Neuman and Di Federico, 2003). Here, we show that the mean value of a multifractal K field also increases with increasing scale or resolution. Iteration level is related to the resolution by $\ell = \frac{1}{b^i}$ or $i = -\log_b(\ell)$, where ℓ is a normalized length scale. Recalling the definition of $D_{q\to\infty}$ in Eq. (13B), we can rewrite Eq. (17) as:

$$K_{\text{eff},i} \approx e^{\alpha \log_b(\ell)} \approx \ell^{2 - D_{q\to\infty}} \tag{18}$$

This remarkably simple expression indicates that the average saturated hydraulic conductivity of a two-dimensional multifractal reservoir increases as a power law with increasing length scale. A similar power law relationship between effective normalized permeability and scale of observation, Eq. (2), was derived previously for geometrical multifractal fields by Saucier (1992a,b). However, the exponent in that relationship was an undefined function of the arbitrary mass fractions used to generate the fields. In contrast, the exponent in Eq. (18) is defined explicitly by $2 - D_{q\to\infty}$, which means that the scaling behavior of the effective hydraulic conductivity is controlled by the maximum generator average mass fraction, $\langle f_{\max,1} \rangle$ (i.e., that part of the generator with the greatest hydraulic conductivity). Since $\langle f_{\max,1} \rangle$ is defined by Eq. (7), the scaling of $K_{\text{eff},i}$ can be inferred directly from knowledge of just p and b. This appears to be a new and potentially powerful result.

5. Summary and research opportunities

We have described a new approach for generating multifractal Sierpinski carpets based on generator average mass fractions calculated using the truncated Binomial distribution with parameters b and p. The generalized dimension versus q functions for such carpets can be computed directly from knowledge of the

Table 4
Results of linear regression analyses between effective saturated hydraulic conductivities from the numerical simulations and those obtained by different averaging techniques ($i = 1$–5)

Numerical	Method	Intercept	Slope	R^2
x-direction	Arithmetic	−0.117	0.988	0.992
	Geometric	0.068	0.834	0.988
	Harmonic	0.211	0.751	0.976
	Perturbation	0.036	0.850	0.992
y-direction	Arithmetic	−0.105	1.040	0.997
	Geometric	0.089	0.877	0.994
	Harmonic	0.240	0.792	0.984
	Perturbation	0.056	0.894	0.997

generator average mass fractions. The D_q functions pass through two at $q=0$, and approach minimum and maximum values as $q \rightarrow \pm\infty$, respectively. The maximum value of D_q is determined by the smallest average mass fraction in the generator, while the minimum value is determined by the largest fraction. The D_q maxima increased dramatically with decreasing p, while the minima decreased slightly.

Average mass fractions at the i−th iteration level were normalized and converted into two-dimensional saturated hydraulic conductivity fields by assuming $K_{j,i} \propto f_{j,i}^{*}$. This approach resulted in increasingly uniform $K_{j,i}$ fields as the iteration level was increased. Since the $K_{j,i}$ of soils and aquifers is rarely uniformly distributed, the exploration of other assumptions such as $K_{j,i} \propto 10^{f_{j,i}^{*}}$ may prove useful.

An approximate analytical expression was derived for the effective saturated hydraulic conductivity of the $K_{j,i}$ fields based on the arithmetic average of the normalized mass fractions. The $K_{\mathrm{eff},i}$ increased with increasing carpet length as a power law with a scaling exponent of $2-D_{q\rightarrow\infty}$. Numerical simulations of flow produced similar increases in $K_{\mathrm{eff},i}$ with increasing length scale.

Further research on two-dimensional saturated hydraulic conductivity fields constructed using other b, p and i values would be valuable. Extension of this approach to three dimensions (i.e., multifractal Menger sponges) should be relatively straightforward. In this study, we controlled lacunarity by choosing a particular arrangement of the generator average mass fractions. Additional numerical simulations of flow in fields based on other arrangements are needed to explore the influence of lacunarity on the scaling of $K_{\mathrm{eff},i}$. Particle tracking could also be employed to investigate the dispersivity of multifractal saturated hydraulic conductivity fields. It may be possible to derive an analytical expression for the dispersivity by studying the variance of these fields, as was done here for the arithmetic average.

Most previous work on multifractals in sub-surface hydrology has focused on stochastic multifractals and Lévy motions. Thus, it is important to be able to relate our results to those obtained using these approaches. One possible way of doing this would be to generate random geometrical multifractals and then analyze their increments using traditional stochastic methods. Future research in this direction may well prove fruitful.

References

Beck, C., Schlögl, F., 1993. Thermodynamics of Chaotic Systems: An Introduction. Cambridge University Press, New York, NY. 286 pp.

Bird, N.R.A., Dexter, A.R., 1997. Simulation of soil water retention using random fractal networks. Eur. J. Soil Sci. 48, 633–641.

Bird, N.R.A., Bartoli, F., Dexter, A.R., 1996. Water retention models for fractal soil structures. Eur. J. Soil Sci. 47, 1–6.

Boufadel, M.C., Lu, S., Molz, F.J., Lavallee, D., 2000. Multifractal scaling of the intrinsic permeability. Water Resour. Res. 36, 3211–3222.

Cawley, R., Mauldin, R.D., 1992. Multifractal decompositions of Moran fractals. Adv. Math. 92, 196–236.

Doughty, C., Karasaki, K., 2002. Flow and transport in hierarchically fractured rock. J. Hydrol. 263, 1–22.

Evertsz, C.J.G., Mandelbrot, B.B., 1992. Multifractal measures. In: Peitgen, H.-O., Jurgens, H., Saupe, D. (Eds.), Chaos and Fractals: New Frontiers of Science. Springer-Verlag, New York, NY, pp. 921–969.

Freund, J.E., 1971. Mathematical Statistics. Prentice-Hall, Inc., Engelwood Cliffs, NJ. 463 pp.

Garrison Jr., J.R., Pearn, W.C., Rosenberg, D.U., 1992. The fractal Menger sponge and Sierpinski carpet as models for reservoir rock/pore systems: I. Theory and image analysis of Sierpinski carpets. In Situ 16, 351–406.

Garrison Jr., J.R., Pearn, W.C., Rosenberg, D.U., 1993. The fractal Menger sponge and Sierpinski carpet as models for reservoir rock/pore systems: II. Image analysis of natural fractal reservoir rocks. In Situ 17, 1–53.

Giménez, D., Rawls, W.J., Lauren, J.G., 1999. Scaling properties of saturated hydraulic conductivity in soil. Geoderma 88, 205–220.

Gouyet, J.-F., 1996. Physics and Fractal Structures. Springer, New York, NY. 234 pp.

Harbaugh, A.W., 1990. A computer program for calculating subregional water budgets using results from the U.S. geological survey modular three-dimensional ground-water flow model. U.S. Geological Survey Open-File Report 90-392. 46 pp.

Harbaugh, A.W., Banta, E.R., Hill, M.C., McDonald, M.G., 2000. MODFLOW-2000, the U.S. geological survey modular ground-water model—user guide to modularization concepts and the ground-water flow process. U.S. Geological Survey Open-File Report 00-92. 121 pp.

King, P.R., 1989. The use of renormalization for calculating effective permeability. Transp. Porous Media 4, 37–58.

Liu, H.H., Molz, F.J., 1997. Multifractal analyses of hydraulic conductivity distributions. Water Resour. Res. 33, 2483–2488.

Mandelbrot, B.B., 1974. Intermittent turbulence in self-similar cascades: divergence of high moments and dimension of the carrier. J. Fluid Mech. 62, 331–358.

Mandlebrot, B.B., 1982. The Fractal Geometry of Nature. W.H. Freeman, New York, NY. 468 pp.

Mandelbrot, B.B., 1989. Multifractal measures, especially for the geophysicist. PAGEOPH 131, 5–42.

Molz, F.J., Rajaram, H., Lu, S., 2004. Stochastic fractal-based models of heterogeneity in subsurface hydrology: origins, applications, limitations, and future research questions. Rev. Geophys. 42, 1002. doi:10.1029/2003RG000126.

Mukhopadhyay, S., Sahimi, M., 2000. Calculation of effective permeabilities of field-scale porous media. Chem. Eng. Sci. 55, 4495–4513.

Neuman, S.P., Di Federico, V., 2003. Multifaceted nature of hydrogeologic scaling and its interpretation. Rev. Geophys. 41, 1014. doi:10.1029/2003RG000130.

Painter, S., Mahinthakumar, G., 1999. Prediction uncertainty for tracer migration in random heterogeneities with multifractal character. Adv. Water Resour. 23, 49–57.

Patil, G.P., 1962. Maximum likelihood estimation for generalized power series distributions and its application to the truncated binomial distribution. Biometrika 49, 227–237.

Perfect, E., 2005. Modeling the primary drainage curve of prefractal porous media. Vadose Zone J. 4, 959–966.

Renard, Ph., de Marsily, G., 1997. Calculating equivalent permeability: a review. Adv. Water Resour. 20, 253–278.

Saucier, A., 1992a. Effective permeability of multifractal porous media. Physica, A 183, 381–397.

Saucier, A., 1992b. Scaling of the effective permeability in multifractal porous media. Physica, A 191, 289–294.

Saucier, A., 1996. Scaling properties of disordered multifractals. Physica, A 226, 34–63.

Shapiro, A.M., Margolin, J., Dolev, S., Ben-Israel, Y., 1997. A graphical-user interface for the U.S. geological survey modular three-dimensional finite-difference ground-water flow model (MODFLOW-96) using Argus numerical environments. U.S. Geological Survey Open-File Report 97-121. 50 pp.

Sukop, M.C., Perfect, E., Bird, N.R.A., 2001. Water retention of prefractal porous media generated with the homogeneous and heterogeneous algorithms. Water Resour. Res. 37, 2631–2636.

Sukop, M.C., van Dijk, G.-J., Perfect, E., van Loon, W.K.P., 2002. Percolation thresholds in 2-dimensional prefractal models of porous media. Transp. Porous Media 48, 187–208.

Tennekoon, L., Boufadel, M.C., Lavalle, D., Weaver, J., 2003. Multifractal anisotropic scaling of hydraulic conductivity. Water Resour. Res. 39 (7), 1193. doi:10.1029/2002WR001645.

Turcotte, D.L., 1997. Fractals and Chaos in Geology and Geophysics, 2nd edition. Cambridge University Press. 398 pp.

Tyler, S., Wheatcraft, S.W., 1990. Fractal processes in soil water retention. Water Resour. Res. 26, 1047–1054.

Veneziano, D., Essiam, A.K., 2003. Flow through porous media with multifractal hydraulic conductivity. Water Resour. Res. 39 (6), 1166. doi:10.1029/2001WR001018.

Veneziano, D., Essiam, A.K., 2004. Nonlinear spectral analysis of flow through multifractal porous media. Chaos, Solitons Fractals 19, 293–307.

Wheatcraft, S.W., Sharp, G.A., Tyler, S.W., 1991. Fluid flow and solute transport in fractal heterogeneous porous media. In: Bear, J., Corapcioglu, M.Y. (Eds.), Transport Processes in Porous Media. Kluwer Academic, Dordrecht, The Netherlands, pp. 695–722.